Research Square

Preprints are preliminary reports that have not undergone peer review.
They should not be considered conclusive, used to inform clinical practice,
or referenced by the media as validated information.

Integrative transcriptomic and single-nucleus analyses identify ZEB1 as a key regulator of ovarian aging in granulosa cells

Jing Ma
The First Affiliated Hospital of Kunming Medical University
Anlai Ming
The First Affiliated Hospital of Kunming Medical University
Ying Wen
The First Affiliated Hospital of Kunming Medical University
Li Tang
The First Affiliated Hospital of Kunming Medical University
Ya Wen
christinewenya@126.com

The First Affiliated Hospital of Kunming Medical University

Research Article

Keywords: Ovarian aging, Granulosa cell heterogeneity, ZEB1, Oxidative stress, Single-cell transcriptomics

Posted Date: April 30th, 2026

DOI: https://doi.org/10.21203/rs.3.rs-9045470/v1

License: This work is licensed under a Creative Commons Attribution 4.0 International License.
Read Full License

Additional Declarations: No competing interests reported.

Abstract

Background

Ovarian aging is characterized by a progressive decline in follicular quantity and quality, in which granulosa cell (GC) dysfunction plays a central role. Although transcriptomic alterations associated with GC aging have been reported, the cellular heterogeneity underlying these changes and the key regulatory mechanisms involved remain incompletely understood.

Methods

We integrated bulk transcriptomic data (GSE232306) and single-cell RNA sequencing data (GSE202601) to systematically investigate aging-associated molecular programs and cellular states in human ovarian granulosa cells. Differential expression analysis, ssGSEA, and weighted gene co-expression network analysis (WGCNA) were applied to identify aging-related pathways and regulatory modules. Single-cell analyses, including AUCell scoring, CytoTRACE, and pseudotime trajectory reconstruction, were used to characterize GC subpopulation dynamics. Key regulatory genes were further validated through functional assays in primary granulosa cells and GC cell lines.

Results

Bulk transcriptomic analysis revealed extensive transcriptional reprogramming in aged granulosa cells, with enrichment of senescence-related pathways and identification of a core aging-associated gene module. Single-cell analysis uncovered pronounced GC heterogeneity and identified a distinct subpopulation, cluster 4, that was preferentially enriched in aged ovaries. This cluster exhibited coordinated activation of ovarian aging–related gene signatures, reduced developmental potential, and a unique differentiation trajectory. Protein–protein interaction analysis highlighted nine hub genes centrally positioned within the cluster 4 regulatory network. Among them, ZEB1 showed strong association with aging-related transcriptional activity. Functional experiments demonstrated that ZEB1 knockdown impaired GC proliferation and increased oxidative stress, supporting its role in maintaining GC homeostasis.

Introduction

Ovarian aging is a fundamental biological process that contributes to the age-dependent decline in female reproductive potential[1,2]. It is characterized by progressive depletion of the follicular pool, reduced oocyte quality, ultimately culminating in reproductive senescence[2]. While oocyte aging has long been considered the primary driver of ovarian decline[3], increasing evidence indicates that dysfunction of ovarian somatic cells, particularly granulosa cells (GCs), plays a critical and often underappreciated role in this process[4,5].

Granulosa cells are essential for follicular development, oocyte maturation, and steroid hormone production[6]. Through gap junction–mediated metabolite exchange and bidirectional paracrine signaling, granulosa cells coordinate oocyte metabolic homeostasis, meiotic progression, and resilience to cellular stress[7,8]. Age-associated alterations in GC proliferation, differentiation capacity, mitochondrial function, and redox balance have been linked to follicular atresia and diminished ovarian reserve[9]. However, most previous studies have treated granulosa cells as a relatively homogeneous population, limiting insight into how specific GC subtypes contribute to ovarian aging.

Advances in transcriptomic profiling have begun to delineate molecular alterations associated with granulosa cell aging[10]. Bulk RNA sequencing analyses have revealed widespread transcriptional remodeling related to cellular stress responses, metabolic reprogramming, and survival–death balance. However, bulk-level measurements average signals across heterogeneous cell populations and therefore cannot resolve whether these age-associated signatures arise uniformly across granulosa cells or are confined to specific cellular states.

More recently, single-cell transcriptomic approaches have uncovered substantial heterogeneity among granulosa cells, identifying distinct functional states linked to proliferation, endocrine responsiveness, and stress adaptation[11]. Nevertheless, the precise GC subpopulations that preferentially exhibit aging-associated features and the regulatory mechanisms sustaining these states remain incompletely defined.

Cellular aging is increasingly understood as a state-dependent process rather than a uniform, cell-autonomous decline[12,13]. In multiple tissues, aging is accompanied by shifts in cell state composition, accumulation of stress-adapted or low-plasticity cell populations, and activation of compensatory transcriptional programs that transiently preserve viability at the cost of functional flexibility[14,15]. Whether similar principles apply to granulosa cells during ovarian aging, and how such states are regulated at the molecular level, remains an open question.

In this study, we combined bulk and single-cell transcriptomic analyses to systematically investigate granulosa cell aging in the human ovary. By integrating differential expression analysis, pathway activity scoring, co-expression network construction, and single-cell trajectory inference, we identified a distinct granulosa cell subpopulation that is preferentially enriched in aged ovaries and exhibits coordinated activation of ovarian aging–related gene programs. Furthermore, we uncovered a ZEB1-centered regulatory network associated with this aging-linked cell state and validated its functional relevance in granulosa cells. Together, our findings provide new insight into the cellular heterogeneity and regulatory mechanisms underlying ovarian aging, offering a focused framework for future mechanistic and translational studies.

Methods

Transcriptomic data processing and normalization (bulk RNA-seq)

Bulk RNA-seq data of human ovarian granulosa cells were obtained from the Gene Expression Omnibus (GEO) database (GSE232306). Samples were classified into young (healthy) and aged groups according to the original dataset metadata. Gene expression matrices were imported into R (version ≥ 4.2.0) for downstream analyses.

Lowly expressed genes were filtered prior to analysis to improve data quality. Expression values were log-transformed where appropriate to stabilize variance across samples. All subsequent analyses were conducted using R and relevant Bioconductor packages.

Single-sample gene set enrichment analysis (ssGSEA)

To characterize pathway-level activity patterns across samples, single-sample gene set enrichment analysis (ssGSEA) was performed using the GSVA package. Curated gene sets were obtained from the Molecular Signatures Database (MSigDB), including hallmark and pathway-related collections.

Normalized expression data were used as input, and enrichment scores were calculated for each gene set in each sample. These scores represent relative pathway activity at the individual-sample level and were subsequently used for comparative and network-based analyses.

Differential expression analysis

Differential expression analysis between aged and young granulosa cell samples was performed to identify aging-associated transcriptional changes. Genes with significant expression differences were defined based on adjusted P values and fold-change thresholds.

Differentially expressed genes (DEGs) were used for downstream functional enrichment analyses and integrated with network-based results to prioritize biologically relevant candidates.

Weighted gene co-expression network analysis (WGCNA)

Weighted gene co-expression network analysis (WGCNA) was conducted using the WGCNA package in R. Genes were ranked by expression variance, and the most variable genes were selected to construct the co-expression network.

An appropriate soft-thresholding power was chosen based on the scale-free topology criterion. An adjacency matrix was constructed and transformed into a topological overlap matrix (TOM), followed by hierarchical clustering to identify gene co-expression modules. Modules with highly similar expression profiles were merged based on eigengene correlation.

Module eigengenes were correlated with ssGSEA-derived pathway enrichment scores and sample traits to identify modules associated with aging-related functional alterations.

Identification of key module genes

Within aging-associated modules, genes were prioritized based on module membership (MM) and gene significance (GS) values. Genes exhibiting high intramodular connectivity and strong associations with aging-related traits were selected for further analysis.

A composite ranking strategy integrating module membership, gene significance, and gene expression abundance was applied to identify representative hub genes within key modules.

Functional enrichment analysis

Kyoto Encyclopedia of Genes and Genomes (KEGG) pathway enrichment analysis was performed using the clusterProfiler package, with gene annotation provided by the org.Hs.eg.db database.

Significantly enriched pathways were identified based on adjusted P values, providing insight into the biological processes underlying aging-associated transcriptional changes in human ovarian granulosa cells.

Single-nucleus RNA sequencing data processing and quality control

Single-nucleus RNA-sequencing (snRNA-seq) data of human ovarian tissue were obtained from GEO (GSE202601). Raw gene–cell count matrices and corresponding metadata were imported into R and analyzed using the Seurat package. Genes detected in at least three nuclei and nuclei expressing a minimum of 200 genes were retained.

Quality control was performed based on the distribution of detected genes, total UMI counts, and mitochondrial transcript proportions. Given the characteristics of snRNA-seq data, filtering thresholds were determined in a data-driven manner. After quality control, 41,470 high-quality nuclei were retained for subsequent analyses.

Data normalization, clustering, and visualization

Filtered snRNA-seq data were normalized using Seurat's log-normalization approach, and highly variable genes were identified. Principal component analysis (PCA) was performed for dimensionality reduction, followed by construction of a shared nearest-neighbor (SNN) graph and unsupervised clustering using the Louvain algorithm (resolution = 0.5).

Uniform Manifold Approximation and Projection (UMAP) was used for two-dimensional visualization of cell clusters.

Cell-type annotation and granulosa cell subclustering

Cell types were annotated based on curated marker gene expression and provided annotations. Major ovarian cell populations were identified, and granulosa cells were extracted for focused downstream analyses. Canonical granulosa cell marker expression was visualized to validate annotation accuracy.

Granulosa cells were reanalyzed independently following the same normalization, scaling, and clustering workflow. Eight granulosa cell subclusters were identified. Both UMAP and t-SNE were used to visualize granulosa cell subpopulations, and cluster distributions were examined across age groups.

Differential expression analysis of granulosa cell subclusters

Differential expression analysis was performed for each granulosa cell subcluster using the FindMarkers function in Seurat with the Wilcoxon rank-sum test. Genes with an absolute log2 fold change > 0.25 and detected in at least 10% of cells were considered significant.

Cluster-specific DEGs were summarized and visualized using volcano plots and dot plots.

AUCell analysis of aging-related gene signatures

AUCell analysis was conducted using the AUCell package to assess aging-related gene-set activity at the single-cell level. Raw count matrices were used to construct gene rankings for each nucleus, and AUC scores were calculated using a predefined ovarian aging-related gene set.

AUCell scores were integrated into the Seurat object metadata and compared across granulosa cell subclusters. Statistical differences were assessed using Kruskal–Wallis and pairwise Wilcoxon rank-sum tests with false discovery rate correction.

Primary granulosa cell isolation and quantitative real-time PCR (qPCR)

Primary human ovarian granulosa cells were isolated from follicular fluid obtained during assisted reproductive procedures. After removal of red blood cells and cellular debris, granulosa cells were collected and cultured under standard conditions. Total RNA was extracted using a commercial RNA isolation reagent according to the manufacturer’s instructions. RNA concentration and purity were assessed spectrophotometrically, and complementary DNA (cDNA) was synthesized using a reverse transcription kit.

Quantitative real-time PCR (qPCR) was performed to assess the expression levels of selected candidate genes, including EP300, FOXO3, and ZEB1. Amplification was conducted using SYBR Green chemistry on

a real-time PCR system. Relative gene expression levels were calculated using the 2^−ΔΔCt method, with housekeeping genes serving as internal controls.

Small interfering RNA (siRNA)–mediated knockdown of ZEB1

To investigate the functional role of ZEB1 in granulosa cells, siRNA-mediated gene silencing was performed in a human granulosa cell line. Cells were transfected with ZEB1-specific siRNA or negative control siRNA using a lipid-based transfection reagent following the manufacturer's protocol. Transfection efficiency and knockdown efficiency were evaluated by qPCR at 24–48 h post-transfection.

Cell proliferation assays

Cell proliferation following ZEB1 knockdown was evaluated using Cell Counting Kit-8 (CCK-8) assays. Transfected cells were seeded into 96-well plates, and CCK-8 reagent was added at the indicated time points. Absorbance was measured at 450 nm to assess cell viability and proliferative capacity.

In parallel, 5-ethynyl-2'-deoxyuridine (EdU) incorporation assays were performed to assess DNA synthesis activity. Cells were incubated with EdU according to the manufacturer's instructions, followed by fixation, permeabilization, and fluorescent labeling. The proportion of EdU-positive cells was quantified using fluorescence microscopy.

Assessment of mitochondrial membrane potential and reactive oxygen species (ROS)

Mitochondrial membrane potential was evaluated using JC-1 staining. Transfected granulosa cells were incubated with JC-1 dye, washed, and analyzed by fluorescence microscopy. Changes in the red-to-green fluorescence ratio were used to reflect alterations in mitochondrial membrane potential.

Intracellular reactive oxygen species (ROS) levels were measured using a fluorescent ROS detection probe. Cells were incubated with the probe under dark conditions, washed to remove excess dye, and imaged using a fluorescence microscope. Fluorescence intensity was quantified to assess relative oxidative stress levels.

Statistical analysis

All experiments were independently repeated at least three times. Quantitative data are presented as mean ± standard deviation (SD). Statistical analyses for experimental data were performed using R or GraphPad Prism. Comparisons between two groups were conducted using Student's t-test, and a two-sided P value < 0.05 was considered statistically significant.

All computational analyses and data visualizations were conducted in R to ensure reproducibility and consistency throughout the analysis workflow.

Results

Transcriptomic profiling identifies aging-associated pathways and key regulatory modules in human ovarian granulosa cells

Using the GEO dataset GSE232306, we first performed differential expression analysis between young (healthy) and aged ovarian granulosa cell samples. A total of 5,174 differentially expressed genes (DEGs) were identified, including 2,294 upregulated and 2,880 downregulated genes in the aged group ($|\log2FC| \geq 1$, adjusted $P < 0.05$), indicating extensive transcriptional reprogramming during ovarian aging (Fig. 1A).

To further characterize aging-related biological activity, senescence-associated gene sets were collected from multiple public databases and ssGSEA enrichment scores were calculated for each sample. Compared with the normal ovarian reserve (NOR) group, the diminished ovarian reserve (DOR) group exhibited consistently higher enrichment scores across Reactome, SASP, GenAge, CSgene, CellAge, GO and KEGG senescence-related signatures (Fig. 1B). Subsequent statistical comparisons identified three significantly altered senescence-related pathways, including GO, KEGG and GenAge gene sets, all of which showed markedly elevated activity in the DOR group ($P < 0.05$), further supporting the enhanced aging-associated molecular phenotype in granulosa cells from older individuals (Fig. 1C).

Based on the DEGs and the three significantly altered ssGSEA pathway scores, weighted gene co-expression network analysis (WGCNA) was performed to construct gene co-expression modules. The resulting clustering dendrogram demonstrated clear module separation and robust network structure (Fig. 1D). Module–trait correlation analysis revealed that the MEblack module exhibited a strong positive association with senescence-related phenotypes, whereas the MEgreenyellow module showed a pronounced negative correlation (Fig. 1E). Notably, the MEblack module displayed significant correlations with multiple aging signatures, including GenAge ($r = 0.55$, $P = 0.07$), GO ($r = 0.72$, $P = 0.008$) and KEGG ($r = 0.85$, $P = 4 \times 10^{-4}$), while MEgreenyellow showed inverse associations with GenAge ($r = -0.63$, $P = 0.03$), GO ($r = -0.83$, $P = 8 \times 10^{-4}$) and KEGG ($r = -0.90$, $P = 8 \times 10^{-5}$) (Fig. 1E).

Functional enrichment analysis of genes within the MEblack module revealed significant involvement in multiple signaling pathways closely related to ovarian function and cellular aging, including the Wnt, TGF-β, PI3K–Akt, mTOR, MAPK and FoxO signaling pathways, as well as pathways associated with cellular senescence, cell cycle regulation, autophagy and apoptosis ($P < 0.05$) (Fig. 1F). These results suggest that the MEblack module may represent a core regulatory network driving age-associated functional alterations in granulosa cells.

To further identify key regulatory hubs, a protein–protein interaction (PPI) network was constructed based on MEblack module genes, and high-density subnetworks were extracted using the MCODE algorithm. Two major clusters were identified: cluster 1 (score = 10.121), containing NOTCH2, ATM,

MBI1, BRAF and FOXO3 as central nodes, and cluster 2 (score = 8.19), enriched for NF1, BIRC6, FRS2 and EML4 (Fig. 1G). These hub genes represent potential regulators linking aging-related signaling pathways with granulosa cell dysfunction.

Finally, genes derived from KEGG senescence-related pathways and high-confidence PPI clusters were integrated to construct a customized ovarian aging-related gene set. ssGSEA analysis demonstrated that the activity score of this gene set was significantly higher in the aged group compared with the young group, further validating its strong association with ovarian aging phenotypes (Fig. 1H).

To further validate the transcriptomic differences observed in aging ovarian granulosa cells, we examined the expression of 124 genes that were significantly upregulated in the DOR group compared with the NOR group. Intergroup comparisons demonstrated a consistent trend of higher expression in DOR samples (Supplementary Fig. 1), confirming that these genes are robustly associated with advanced ovarian age. Statistical analysis using two-sided t-tests indicated that the majority of these genes were significantly elevated in the DOR group (*P < 0.05, **P < 0.01), supporting the overall enrichment pattern observed in the aging-associated pathways from our prior differential expression and WGCNA analyses (Fig. 1).

Single-cell transcriptomic profiling reveals granulosa cell heterogeneity and age-associated subpopulation dynamics in human ovaries

To dissect cellular heterogeneity in human ovarian granulosa cells (GCs), we analyzed the scRNA-seq dataset GSE202601. UMAP visualization of all ovarian cells identified eight major cell types, including epithelial cells (EpiC), smooth muscle cells (SMC), T cells (TC), stromal cells (SC), immune cells (IC), granulosa cells (GC), lymphatic endothelial cells (LEC), and blood endothelial cells (BEC) (Fig. 2A). GC-specific marker genes, including FOXL2, AMH, FST, INHA, INHBA, CYP19A1, CCND2, GJA1, ESR2, and HSD17B1, were predominantly expressed in the GC population, confirming cell type annotation (Fig. 2B).

Focusing on GCs, we extracted this subset and performed re-clustering and UMAP dimensionality reduction, revealing eight distinct GC subclusters (Fig. 2C). Mapping donor age onto the GC UMAP revealed a clear age-related distribution pattern: cells from young ovaries (ovary23) were enriched in clusters 0, 2, 3, 5, and 7, whereas cells from older donors (ovary51, 52, 54) mainly occupied cluster 4, ovary27 was distributed across clusters 1 and 6, and ovary29 was distributed across clusters 3(Fig. 2D). Consistently, grouping by young versus old samples showed that GC cells from older individuals were predominantly localized to cluster 4, while younger cells were distributed across multiple other clusters (Fig. 2E). Quantitative comparison of GC cell proportions between groups demonstrated a lower abundance of GCs in the aged samples compared with young samples (Fig. 2F).

Differential expression analysis across the eight GC clusters identified cluster-specific genes, with the number of upregulated and downregulated genes exceeding 350 in each cluster, and in some clusters reaching nearly 1,900 genes (Fig. 2G). The top five marker genes for each cluster highlighted

subpopulation-specific transcriptional programs: cluster 0 expressed AL031599.1, GABRG3, CYP51A1-AS1, SPINT4, and AC090673.1; cluster 1 expressed HSPA6, HSPE1-MOB4, BAG3, DNAJA4, and HSPH1; cluster 2 expressed HRASLS5, FAM166B, CLIC5, EREG, and CD274; cluster 3 expressed MTRNR2L1, ADGRL3, AP002991.1, SNTG2, and AC007221.2; cluster 4 expressed MSC-AS1, TMEM132C, EPB41L3, MEIS1, and TOX; cluster 5 expressed MGP, TAGLN, S100A6, APRT, and PRDX5; cluster 6 expressed CDCA2, TICRR, TTK, MKI67, and UBE2C; and cluster 7 expressed PTCH2, AL355581.1, MELK, SMAGP, and AC090531.1 (Fig. 2H).

KEGG pathway enrichment analysis of cluster-specific DEGs revealed that distinct GC subpopulations were associated with unique biological processes: cluster 0 was enriched for protein processing in the endoplasmic reticulum; cluster 1 for endocytosis; cluster 2 for protein processing in the endoplasmic reticulum and autophagy; cluster 3 for endocytosis, ubiquitin-mediated proteolysis, and protein processing in the endoplasmic reticulum; cluster 4 for endocytosis and protein processing in the endoplasmic reticulum; cluster 5 for protein processing in the endoplasmic reticulum, endocytosis, and ubiquitin-mediated proteolysis; and cluster 6 for cell cycle, endocytosis, and ubiquitin-mediated proteolysis (Fig. 2I). These findings demonstrate that human ovarian GCs are transcriptionally heterogeneous, and that specific subpopulations exhibit distinct age-associated distributions and functional states, providing a cellular framework to investigate mechanisms underlying ovarian aging.

AUCell-based activity profiling reveals cluster 4 as a granulosa cell subpopulation enriched for ovarian aging–related gene signatures

To evaluate the activity of the customized ovarian insufficiency–related gene set at the single-cell level, AUCell analysis was performed across all granulosa cells. The global AUCell score distribution showed a clear separation between activated and non-activated cells, with a threshold of approximately 0.161, identifying 888 activated cells, accounting for 54.8% of the total GC population (Fig. 3A).

We next compared the proportion of activated cells across the eight GC clusters. Cluster 3 exhibited the highest activation ratio (0.88), followed by cluster 6 (0.76), cluster 1 (0.75), and cluster 4 (0.63), indicating marked heterogeneity in ovarian aging–related pathway activity among GC subpopulations (Fig. 3B). Consistently, statistical comparison of AUCell scores across clusters revealed significant differences (Kruskal–Wallis test, $P < 2.2 \times 10^{-16}$), with cluster 3 showing the highest overall activity, followed by clusters 1, 6, and 4 (Fig. 3C).

Visualization of AUCell scores on the UMAP embedding further demonstrated that high-activity cells were spatially enriched in clusters 1, 3, 4, and 6, forming distinct functional regions within the GC landscape (Fig. 3D). Notably, although cluster 3 showed the strongest activation signal, cluster 4 was of particular interest because it was previously identified as the predominant cluster enriched in aged ovarian samples (Fig. 2E). Therefore, cluster 4 represents a GC subpopulation that simultaneously exhibits age-associated accumulation and activation of ovarian insufficiency–related molecular programs (Fig. 3E).

To further characterize the molecular features of this aging-associated subpopulation, cluster 4 cells were stratified into high- and low-AUCell activity groups based on score distribution density (Fig. 3F). Differential expression analysis between these two groups identified 1,191 upregulated and 17 downregulated genes in the high-activity subgroup ($P < 0.05$, $|log2FC| > 0.25$), indicating extensive transcriptional remodeling associated with elevated ovarian aging signature activity (Fig. 3G). Hypergeometric testing confirmed a highly significant enrichment of ovarian insufficiency–related genes among the differentially expressed genes ($P = 5.66 \times 10^{-26}$).

Intersection analysis between the DEGs and the customized ovarian insufficiency gene set (124 genes) identified 42 overlapping core genes (Fig. 3H). These genes, including ZEB1, EP300, FOXO3, MTOR, NOTCH2, NF1, BRAF, JAK1, EGFR, BMPR2, GJA1, and SP1, displayed consistently higher expression in high-AUCell cluster 4 cells, as shown in the dot plot visualization (Fig. 3I). Importantly, AUCell scoring based on the 42-gene core signature across all GC clusters demonstrated a significant heterogeneity of activation states among subpopulations (Kruskal–Wallis test, $P < 2.2 \times 10^{-16}$). Notably, cluster 4 exhibited a significantly elevated activation pattern compared with several other clusters, indicating its potential involvement in ovarian aging–associated molecular alterations (Fig. 3J).

Collectively, these results demonstrate that cluster 4 represents a distinct granulosa cell subpopulation characterized by age-associated accumulation and coordinated activation of ovarian insufficiency–related gene programs, providing a focused cellular context for downstream functional validation of key regulatory genes.

Developmental Potential Heterogeneity of Granulosa Cell Subpopulations Revealed by CytoTRACE

To characterize the developmental potential of granulosa cells (GCs) and its relationship with ovarian aging–related molecular programs, CytoTRACE analysis was performed on GC populations. Visualization of CytoTRACE scores on the UMAP revealed pronounced heterogeneity in developmental potential across GC subclusters (Fig. 4A). Quantitative comparison showed that CytoTRACE scores varied significantly among clusters, with cluster2, cluster0, and cluster7 exhibiting relatively higher developmental potential, whereas cluster4 displayed comparatively lower CytoTRACE scores (Fig. 4B).

We next examined the association between cellular developmental potential and the activation of the core 42-gene ovarian aging signature. Spearman correlation analysis demonstrated cluster-specific relationships between CytoTRACE scores and Core 42 Genes AUCell scores (Fig. 4C). Significant positive correlations were observed in cluster1 ($\rho = 0.44$, $p = 2.18 \times 10^{-14}$), cluster3 ($\rho = 0.33$, $p = 5.71 \times 10^{-7}$), and cluster4 ($\rho = 0.30$, $p = 6.1 \times 10^{-6}$), indicating that variations in developmental potential within these subpopulations were closely associated with the activation of ovarian aging–related gene programs. In contrast, no significant correlations were detected in cluster6 or cluster7, with cluster6 showing a weak negative trend.

Collectively, these results suggest that the relationship between GC developmental potential and ovarian aging–associated gene activation is highly subpopulation-specific rather than uniform across all GC clusters. Notably, despite exhibiting relatively lower developmental potential, cluster4 showed a significant association between CytoTRACE scores and the core ovarian aging signature, implying that this subpopulation may represent a distinct functional state linked to ovarian aging–related molecular alterations.

Pseudotime Trajectory Analysis Reveals Distinct Differentiation Paths and Core Gene Activation Dynamics in Granulosa Cells

Using Monocle3, we reconstructed the pseudotemporal differentiation trajectories of granulosa cells to investigate lineage relationships and dynamic molecular changes during cellular progression (Fig. 5A). The trajectory analysis partitioned GC cells into three major differentiation compartments. The first compartment comprised clusters 0, 2, 5, and 7, with cluster 0 positioned at the putative root state and bifurcating toward clusters 7 and 2 along two distinct branches. The second compartment was characterized by cluster 4, which formed an independent differentiation trajectory, suggesting a unique developmental route distinct from other GC subpopulations. The third compartment included clusters 1, 3, and 6, originating from cluster 1 and diverging toward clusters 3 and 6 along two separate branches.

To further explore the distribution of ovarian aging–related molecular activity along the differentiation continuum, the AUCell score derived from the core 42-gene signature was mapped onto the pseudotime trajectory (Fig. 5B). Cells with higher AUCell scores were predominantly enriched in the right-side compartments of the trajectory, particularly within clusters 4, 1, 3, and 6, indicating enhanced activation of ovarian aging–associated gene programs in these differentiation states.

Next, we examined the dynamic expression patterns of 20 key genes selected based on their high expression in cluster 4. Pseudotime expression analysis revealed that these genes including ATG2B, CTSO, EP300, LAMA2, COL4A5, FOXO3, FRMD6, FRS2, FBN1, HIPK3, MTOR, JAK1, GNG12, ZEB1, PARP4, NEO1, MAP3K20, PTPN13, RPS6KA3, and SP1 exhibited the highest expression levels at early pseudotime states corresponding to cluster 0, followed by distinct decreasing trajectories across downstream clusters (Fig. 5C). Although the overall trend was a gradual decline, individual genes displayed heterogeneous expression dynamics, with some showing transient increases before subsequent downregulation, reflecting complex regulatory patterns during GC differentiation.

Functional enrichment analysis of these 20 key genes using KEGG pathway analysis identified multiple biological processes closely related to ovarian aging and cellular stress responses (Fig. 5D). Notably, significantly enriched pathways included focal adhesion, mTOR signaling, FoxO signaling, autophagy, AMPK signaling, cellular senescence, apoptosis, PI3K–Akt signaling, MAPK signaling, and TGF-β signaling pathways (all $p < 0.05$), highlighting the involvement of these genes in metabolic regulation, survival signaling, and age-associated cellular remodeling.

Consistent with KEGG results, Metascape analysis further revealed that these genes were organized into interconnected functional modules related to receptor tyrosine kinase signaling, interleukin-mediated signaling, integrin pathways, apoptosis, cell morphogenesis, protein phosphorylation, and inflammatory responses (Fig. 5E). The integrated pathway–protein interaction network underscores the coordinated regulation of signaling, structural remodeling, and stress response programs during granulosa cell differentiation and ovarian aging.

Identification and Expression Characterization of Core Regulatory Genes in Cluster 4

To further refine the key regulators underlying the molecular features of cluster 4, we constructed a protein–protein interaction (PPI) network based on the 20 cluster 4–associated genes identified from pseudotime and expression analyses (Fig. 6A). The resulting PPI network revealed extensive interactions among these genes, indicating coordinated regulation at the protein level. Network topology analysis highlighted nine genes MTOR, EP300, FOXO3, JAK1, ZEB1, HIPK3, SP1, RPS6KA3, and FRS2 as highly connected nodes, suggesting their potential roles as central regulators within the cluster 4 gene network.

To evaluate the relationship between these nine core genes and ovarian aging–associated transcriptional activity, we assessed the correlation between their expression levels and the AUCell scores derived from the core 42-gene signature across GC clusters. Spearman correlation analysis revealed that the expression of these genes exhibited cluster-specific correlations with the AUCell score. Notably, all nine genes showed significant positive correlations in cluster 4 (Fig. 6B).These results indicate that the activation of the core ovarian aging gene program is closely associated with the expression of these hub genes, particularly within cluster 4.

We next examined the spatial expression patterns of the nine core genes at the single-cell level. UMAP visualization revealed that these genes were preferentially expressed in specific GC subpopulations, with pronounced enrichment in cluster 4 (Fig. 6C). Consistently, dot plot analysis of average gene expression across clusters confirmed that all nine genes exhibited relatively higher expression levels in cluster 4 compared with other GC clusters (Fig. 6D).

Together, these results demonstrate that the nine hub genes identified through PPI network analysis are not only centrally positioned within the cluster 4 regulatory network but also display coordinated expression patterns and strong associations with ovarian aging–related gene activation. This integrative evidence supports their potential roles as key molecular drivers contributing to the distinct transcriptional and functional characteristics of cluster 4 granulosa cells.

ZEB1 regulates proliferation, oxidative stress, and mitochondrial function in ovarian granulosa cells

To experimentally validate the bioinformatic findings and investigate the functional role of ZEB1 in ovarian granulosa cells, we first examined the expression levels of EP300, FOXO3, and ZEB1 in primary

granulosa cells isolated from follicular fluid of young and aged donors. Quantitative real-time PCR analysis showed that the mRNA expression of all three genes was significantly lower in granulosa cells from the aged group compared with those from the young group, indicating an age-associated downregulation of these genes (Fig. 7A).

Based on its strong association with ovarian aging–related transcriptional activity, ZEB1 was selected for further functional characterization. Efficient knockdown of ZEB1 was achieved in a granulosa cell line using siRNA, as confirmed by qPCR analysis (Fig. 7B). Functional assays demonstrated that ZEB1 silencing significantly suppressed granulosa cell proliferation. CCK-8 assays revealed a marked reduction in relative cell viability in the ZEB1 siRNA group compared with the negative control group (Fig. 7C). Consistently, EdU incorporation assays showed a significantly decreased proportion of EdU-positive cells following ZEB1 knockdown, further indicating impaired DNA synthesis and proliferative capacity (Fig. 7D).

In addition to its effects on cell proliferation, ZEB1 knockdown influenced mitochondrial function and oxidative stress. JC-1 staining revealed a decrease in mitochondrial membrane potential in ZEB1-deficient cells; however, this change did not reach statistical significance (Fig. 7E). In contrast, intracellular reactive oxygen species (ROS) levels were significantly increased upon ZEB1 silencing, as evidenced by enhanced DHE fluorescence intensity, indicating elevated oxidative stress (Fig. 7F).

Collectively, these results demonstrate that ZEB1 plays an important role in maintaining granulosa cell proliferative activity and redox homeostasis, and its downregulation contributes to impaired cell growth and increased oxidative stress, supporting a functional role for ZEB1 in ovarian granulosa cell aging.

Discussion

Ovarian aging is a complex and heterogeneous process that involves progressive functional decline of granulosa cells (GCs), ultimately leading to impaired folliculogenesis and reduced reproductive potential[16–18]. Although age-related transcriptional changes in GCs have been reported in bulk and single-cell studies, the specific GC subpopulations that preferentially exhibit aging-associated features and their underlying regulatory mechanisms remain incompletely understood. In this study, we identify a distinct GC subpopulation, cluster 4, that is closely associated with ovarian aging and further delineate a ZEB1-centered regulatory axis that may contribute to the maintenance of GC homeostasis during this process.

Cluster 4 represents an aging-associated granulosa cell subpopulation

Ovarian aging is increasingly recognized as a process driven not only by cumulative molecular damage but also by progressive alterations in granulosa cell state composition[19,20]. Single-cell studies have demonstrated that granulosa cells exist along a continuum of functional states rather than discrete

developmental stages, spanning proliferative, metabolically active, and stress-adapted phenotypes. Within this framework, aging may preferentially promote the emergence or persistence of specific GC states that are less capable of supporting follicular growth.

The identification of cluster 4 as a distinct GC subpopulation associated with ovarian aging suggests that aging-related transcriptional changes are spatially and functionally constrained to a defined cellular context. Rather than reflecting a generalized decline across all granulosa cells, ovarian aging may involve a shift toward GC states characterized by reduced plasticity and increased stress responsiveness. Such state-specific vulnerability has been reported in other aging tissues, where terminally differentiated or stress-adapted cell populations accumulate and contribute disproportionately to tissue dysfunction.

From a developmental standpoint, the reduced differentiation potential observed in cluster 4 is particularly informative. Granulosa cell function relies on the ability to dynamically transition between proliferative and differentiated states in response to endocrine and paracrine cues. Loss of this flexibility can compromise follicular responsiveness to gonadotropins and disrupt oocyte–somatic cell communication. In this regard, cluster 4 may represent a GC state that has crossed a functional threshold, beyond which adaptive responses to physiological signals are impaired. This interpretation aligns with models of ovarian aging proposing that follicular attrition is driven not solely by oocyte loss, but also by the progressive failure of supporting somatic cells.

Importantly, positioning cluster 4 within this conceptual framework helps reconcile disparate observations from previous studies. Aging-associated transcriptional signatures detected in bulk GC analyses may largely reflect the increased representation or transcriptional dominance of this specific subpopulation, rather than uniform molecular remodeling across all granulosa cells. Thus, cluster 4 provides a cellular explanation for how localized state transitions can give rise to global aging phenotypes at the tissue level.

Aging-associated transcriptional programs converge in cluster 4

At the molecular level, ovarian aging is characterized by the coordinated activation of pathways governing cellular stress responses, metabolic adaptation, and survival–death decisions. Pathways such as mTOR, FoxO, AMPK, TGF-β, and PI3K–Akt have been repeatedly implicated in GC aging[21–23], yet their integration within specific cellular states has remained unclear. The preferential enrichment of these pathways within cluster 4 suggests that aging-associated signaling is not randomly distributed but converges within a GC subpopulation predisposed to functional decline.

Notably, many of the pathways enriched in cluster 4 regulate the balance between anabolic growth and stress resistance. For example, dysregulated mTOR and AMPK signaling reflects altered energy sensing[24], while FoxO and TGF-β pathways are central to oxidative stress responses, cell cycle control, and apoptosis [25]. The co-activation of these pathways is consistent with a GC state attempting to maintain survival under chronic stress at the expense of proliferative and differentiation capacity. Such

trade-offs are a recognized feature of cellular aging and may represent an adaptive but ultimately maladaptive response in the ovarian microenvironment.

In addition, enrichment of ECM-related and focal adhesion pathways in cluster 4 highlights potential alterations in cell–matrix interactions. Granulosa cells rely on intact ECM signaling to maintain follicular architecture and transmit mechanical and biochemical cues essential for oocyte support[26–28]. Disruption of these interactions has been linked to follicular atresia and impaired steroidogenesis[29]. The convergence of ECM remodeling, stress signaling, and senescence-related pathways within cluster 4 suggests that this subpopulation may contribute to ovarian aging by simultaneously compromising both intracellular homeostasis and intercellular communication.

Collectively, these observations support a model in which cluster 4 functions as a molecular hub where multiple aging-associated pathways intersect. Rather than acting independently, these pathways may form a coordinated network that stabilizes a low-plasticity, stress-adapted GC state, thereby accelerating functional decline of the follicular unit.

ZEB1 as a key regulator linking cluster 4 to granulosa cell aging

Within the regulatory network associated with cluster 4, ZEB1 emerges as a central transcriptional regulator with important implications for granulosa cell state maintenance under aging-related stress. Although ZEB1 has been extensively studied in the context of epithelial–mesenchymal transition[30,31], increasing evidence suggests that its biological functions extend beyond lineage plasticity to include regulation of cellular homeostasis[32–34], stress adaptation, and transcriptional robustness in differentiated cells[34].

Granulosa cells require tight coordination between proliferation, differentiation, and survival to sustain follicular development and oocyte competence[35,36]. Transcription factors governing this balance are therefore critical determinants of follicular lifespan. The preferential association of ZEB1 with cluster 4 suggests that its activity is not uniformly required across all GC states, but instead becomes particularly relevant in subpopulations experiencing elevated stress and reduced developmental flexibility. This state-dependent engagement is consistent with emerging models of aging, in which regulatory factors are selectively activated to stabilize vulnerable cellular states rather than to promote growth or differentiation.

Importantly, functional perturbation of ZEB1 led to reduced proliferative capacity and increased oxidative stress in granulosa cells, two hallmark features of ovarian aging. Oxidative stress is a well-established driver of follicular atresia[37], contributing to mitochondrial dysfunction, DNA damage [38], and impaired steroidogenic support[39]. The observed increase in reactive oxygen species following ZEB1 depletion suggests that ZEB1 may participate in transcriptional programs that buffer oxidative stress and preserve

cellular viability. Rather than acting as a classical anti-aging factor, ZEB1 may function to delay the functional collapse of granulosa cells by maintaining redox balance and limiting stress-induced damage.

Notably, the effects of ZEB1 interference were more pronounced at the level of proliferation and oxidative stress than mitochondrial membrane potential, implying that ZEB1 primarily influences early stress-adaptive responses rather than terminal mitochondrial failure. This distinction supports a model in which ZEB1 contributes to sustaining a compensatory GC state under chronic stress conditions, consistent with the transcriptional features observed in cluster 4. Such a role aligns with studies in other tissues showing that ZEB1 and related transcription factors act as transcriptional stabilizers, preventing abrupt loss of cell identity under adverse conditions.

Taken together, these findings support a context-dependent role for ZEB1 in ovarian aging. Rather than functioning as a universal regulator across all granulosa cells, ZEB1 appears to exert its effects predominantly within aging-associated GC states, where the balance between survival and functional competence is particularly fragile. By stabilizing stress-adaptive transcriptional programs, ZEB1 may transiently preserve granulosa cell viability while simultaneously marking a cellular state that is predisposed to functional decline. This dual role positions ZEB1 as a key molecular link between granulosa cell stress adaptation and ovarian aging progression.

Implications and perspectives

By integrating single-cell trajectory analysis, transcriptional activity scoring, and functional validation, this study provides a refined view of granulosa cell aging at both the cellular and molecular levels. The identification of cluster 4 as an aging-associated GC subpopulation, together with the characterization of a ZEB1-centered regulatory axis, advances current understanding of ovarian aging beyond descriptive gene expression changes.

These findings have potential implications for the development of targeted strategies aimed at preserving GC function and delaying ovarian aging. Future studies will be required to determine whether modulation of ZEB1 or cluster 4–associated pathways can ameliorate age-related ovarian decline in vivo and whether similar aging-associated GC states are conserved across species. More broadly, our work underscores the importance of resolving cellular heterogeneity when investigating complex reproductive aging processes.

Conclusion

Our integrative analysis reveals that human ovarian granulosa cells exhibit pronounced transcriptional and functional heterogeneity during aging. A distinct subpopulation, cluster 4, is preferentially enriched in aged ovaries and shows coordinated activation of ovarian aging–related gene programs. Nine hub genes, including EP300, FOXO3, and ZEB1, were identified as central regulators within this subpopulation, and experimental validation demonstrated that ZEB1 contributes to granulosa cell

proliferation and redox homeostasis. These findings highlight key molecular drivers underlying granulosa cell aging and provide a focused cellular context for further functional studies.

Declarations

Author Contributions

Ya Wen contributed to conceptualization, resources, data curation, writing–original draft preparation, writing–review and editing, project administration, and funding acquisition. Anlai Min contributed to methodology, software, formal analysis, and visualization. Jing Ma contributed to validation, investigation, and writing–original draft preparation. Ying Wen contributed to visualization. Li Tang contributed to supervision and writing–review and editing.

Acknowledgments

Not applicable.

Data Availability Statement

All the data analyzed in this study were obtained from publicly available repositories (GEO database: GSE232306, GSE202601).

Conflicts of Interest

The authors have no relevant financial or non-financial interests to dis-close.

Funding

This work was supported by the National Natural Science Foundation of China (Grant No. 82360298), the 535 Talent Project of the First Affiliated Hospital of Kunming Medical University (Grant No. 2023535Q12), and the First-Class Discipline Team of Kunming Medical University (Grant No. 2024XKTDTS02).

Patient consent for publication

Written informed consent for publication was obtained from all patients included in this study.

References

1. Hirano M, et al. Ovarian aging: pathophysiology and recent developments in maintaining ovarian reserve. Front Endocrinol. 2025;16:1619516.
2. Wu J, et al. Aging conundrum: A perspective for ovarian aging. Front Endocrinol. 2022;13:952471.
3. Ahmed TA et al. Oocyte aging: the role of cellular and environmental factors and impact on female fertility. Cell Biology Translational Med 8: Stem Cells Regenerative Med, 109–23 (2019).

4. Liu L, Fang Y. The Role of Ovarian Granulosa Cells Related-ncRNAs in Ovarian Dysfunctions: Mechanism Research and Clinical Exploration. Reproductive Sci, 1–23 (2025).
5. Chauvin S. Role of Granulosa Cell Dysfunction in Women Infertility Associated with Polycystic Ovary Syndrome and Obesity. Biomolecules. 2025;15:923.
6. Cavalcanti GS, et al. Granulosa cells and follicular development: a brief review. Revista da Associação Médica Brasileira. 2023;69:e20230175.
7. Zhu Y, Zhu H, Wu P. Gap junctions in polycystic ovary syndrome: Implications for follicular arrest. Dev Dyn. 2024;253:882–94.
8. Pei Z, Deng K, Xu C, Zhang S. The molecular regulatory mechanisms of meiotic arrest and resumption in Oocyte development and maturation. Reproductive Biology Endocrinol. 2023;21:90.
9. Kobayashi H, Yoshimoto C, Matsubara S, Shigetomi H, Imanaka S. Altered energy metabolism, mitochondrial dysfunction, and redox imbalance influencing reproductive performance in granulosa cells and oocyte during aging. Reproductive Sci. 2024;31:906–16.
10. Zhao H, Wang Y, Yang Y. Follicular development and ovary aging: single-cell studies. Biol Reprod. 2023;109:390–407.
11. Wang S, et al. Single-cell transcriptomic atlas of primate ovarian aging. Cell. 2020;180:585–600.
12. López-Otín C, Blasco MA, Partridge L, Serrano M, Kroemer G. Hallmarks of aging: An expanding universe. Cell. 2023;186:243–78.
13. Cohn RL, Gasek NS, Kuchel GA, Xu M. The heterogeneity of cellular senescence: insights at the single-cell level. Trends Cell Biol. 2023;33:9–17.
14. Tam LM, Bushnell T. Deciphering the aging process through single-cell cytometric technologies. Cytometry A. 2024;105:621–38. https://doi.org/10.1002/cyto.a.24852.
15. Wechter N, et al. Single-cell transcriptomic analysis uncovers diverse and dynamic senescent cell populations. Aging. 2023;15:2824–51. https://doi.org/10.18632/aging.204666.
16. Alberico HC, Woods DC. Role of granulosa cells in the aging ovarian landscape: a focus on mitochondrial and metabolic function. Front Physiol. 2022;12:800739.
17. Camaioni A, et al. The process of ovarian aging: it is not just about oocytes and granulosa cells. J Assist Reprod Genet. 2022;39:783–92.
18. Tatone C, Amicarelli F. The aging ovary—the poor granulosa cells. Fertil Steril. 2013;99:12–7.
19. Wang X, Wang L, Xiang W. Mechanisms of ovarian aging in women: a review. J Ovarian Res. 2023;16:67. https://doi.org/10.1186/s13048-023-01151-z.
20. Liu X, Zhao Y, Feng Y, Wang S, Zhang J. Ovarian Aging: Mechanisms, Age-Related Disorders, and Therapeutic Interventions. *MedComm (*2020) 6, e70481 (2025). https://doi.org/10.1002/mco2.70481
21. Kim DH, et al. Organ-differential Roles of Akt/FoxOs Axis as a Key Metabolic Modulator during Aging. Aging Dis. 2021;12:1713–28. https://doi.org/10.14336/ad.2021.0225.

22. Vidović T, Ewald CY. Longevity-Promoting Pathways and Transcription Factors Respond to and Control Extracellular Matrix Dynamics During Aging and Disease. Front Aging. 2022;3:935220. https://doi.org/10.3389/fragi.2022.935220.
23. Zhu X, et al. Mechanistic study on the role of multi-pathway autophagy in ovarian aging: literature review. Apoptosis. 2025;30:2694–721. https://doi.org/10.1007/s10495-025-02181-2.
24. Sukumaran A, Choi K, Dasgupta B. Insight on Transcriptional Regulation of the Energy Sensing AMPK and Biosynthetic mTOR Pathway Genes. Front Cell Dev Biol. 2020;8:671. https://doi.org/10.3389/fcell.2020.00671.
25. Hameedaldeen A, Liu J, Batres A, Graves GS, Graves DT. FOXO1, TGF-β regulation and wound healing. Int J Mol Sci. 2014;15:16257–69. https://doi.org/10.3390/ijms150916257.
26. Wang H, Yang L. Ovarian Mechanobiology: Understanding the Interplay Between Mechanics and Follicular Development. Cells. 2025;14. https://doi.org/10.3390/cells14050355.
27. Fiorentino G, et al. Biomechanical forces and signals operating in the ovary during folliculogenesis and their dysregulation: implications for fertility. Hum Reprod Update. 2023;29:1–23. https://doi.org/10.1093/humupd/dmac031.
28. Woodruff TK, Shea LD. The role of the extracellular matrix in ovarian follicle development. Reprod Sci. 2007;14:6–10. https://doi.org/10.1177/1933719107309818.
29. Voros C, et al. Oxidative Stress and SIRT1-Nrf2 Anti-Ferroptotic Pathways in Granulosa Cells: A Molecular Key to Follicular Atresia and Ovarian Aging. Int J Mol Sci. 2026;27. https://doi.org/10.3390/ijms27020950.
30. Manfioletti G, Fedele M. Epithelial-Mesenchymal Transition (EMT) 2021. Int J Mol Sci. 2022;23. https://doi.org/10.3390/ijms23105848.
31. Huang Z, Zhang Z, Zhou C, Liu L, Huang C. Epithelial-mesenchymal transition: The history, regulatory mechanism, and cancer therapeutic opportunities. MedComm (2020). 2022;3:e144. https://doi.org/10.1002/mco2.144.
32. Wang Y, et al. The transcription factor Zeb1 controls homeostasis and function of type 1 conventional dendritic cells. Nat Commun. 2023;14:6639. https://doi.org/10.1038/s41467-023-42428-7.
33. Zhang Y, et al. Expression and Function of ZEB1 in the Cornea. Cells. 2021;10. https://doi.org/10.3390/cells10040925.
34. Drápela S, Bouchal J, Jolly MK, Culig Z, Souček K. ZEB1: A Critical Regulator of Cell Plasticity, DNA Damage Response, and Therapy Resistance. Front Mol Biosci. 2020;7:36. https://doi.org/10.3389/fmolb.2020.00036.
35. Chen Y, Wang S, Zhang C. The Differentiation Fate of Granulosa Cells and the Regulatory Mechanism in Ovary. Reprod Sci. 2025;32:1414–26. https://doi.org/10.1007/s43032-024-01682-w.
36. Alam MH, Miyano T. Interaction between growing oocytes and granulosa cells in vitro. Reprod Med Biol. 2020;19:13–23. https://doi.org/10.1002/rmb2.12292.

37. Shen YH, Peng S, Zhu T, Shen MJ. Mechanisms of Granulosa Cell Programmed Cell Death and Follicular Atresia in Polycystic Ovary Syndrome. Physiol Res. 2025;74:31–40. https://doi.org/10.33549/physiolres.935485.
38. Chainy GBN, Sahoo DK. Hormones and oxidative stress: an overview. Free Radic Res. 2020;54:1–26. https://doi.org/10.1080/10715762.2019.1702656.
39. Zaidi SK, et al. SOD2 deficiency-induced oxidative stress attenuates steroidogenesis in mouse ovarian granulosa cells. Mol Cell Endocrinol. 2021;519:110888. https://doi.org/10.1016/j.mce.2020.110888.

Tables

Table 1 is available in the Supplementary Files section.

Figures

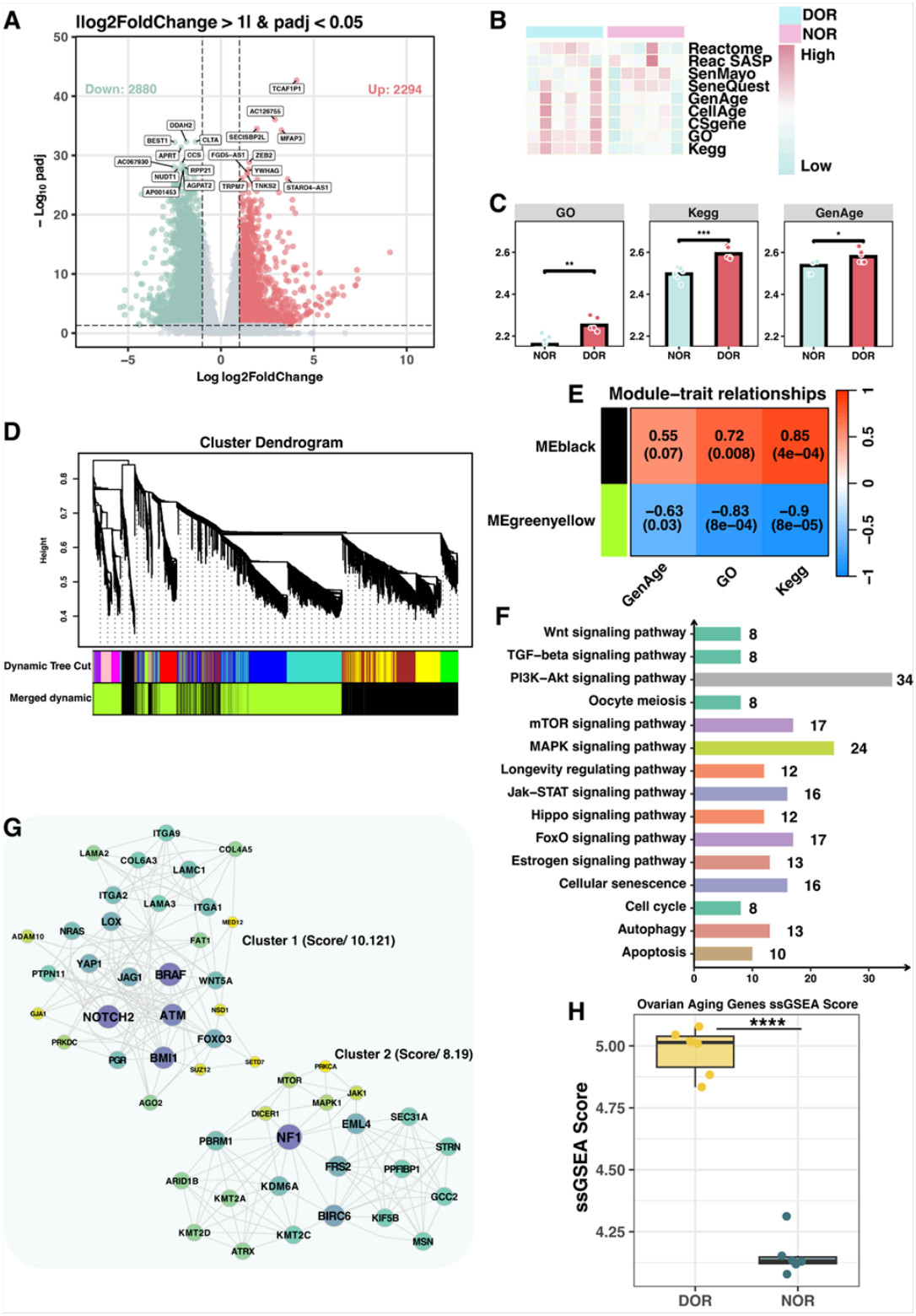


Figure 1

Construction of a custom ovarian aging gene set at the bulk transcriptomic level.

A. Differential expression analysis: Transcriptomic comparison between healthy (young) and aged ovarian granulosa cell samples from GEO dataset GSE232306 to identify differentially expressed genes (DEGs).

B. Aging pathway scoring: ssGSEA scores were calculated for aging-related gene sets obtained from public databases to assess pathway activity in each sample.

C. Group significance testing: Comparison of ssGSEA scores between young and aged groups, identifying three significantly altered pathways ($p < 0.05$).

D. WGCNA module construction: Weighted gene co-expression network analysis was performed using DEGs with the three significant ssGSEA pathway scores as phenotypes; cluster dendrogram of gene modules is shown.

E. Module-trait relationship analysis: Correlations between module eigengenes and phenotypes were calculated, and MEblack module exhibited high correlation with aging-related traits.

F. Functional enrichment analysis: KEGG pathway enrichment of MEblack module genes; significant pathways are shown ($p < 0.05$).

G. Protein-protein interaction network: PPI network of MEblack module genes was constructed, and top two high-density clusters were identified using Cytoscape MCODE.

H. Validation of the custom ovarian aging gene set: KEGG pathway genes and high-density PPI cluster genes were integrated to form a custom gene set. ssGSEA scores demonstrated significantly higher activation in aged samples compared with young samples.

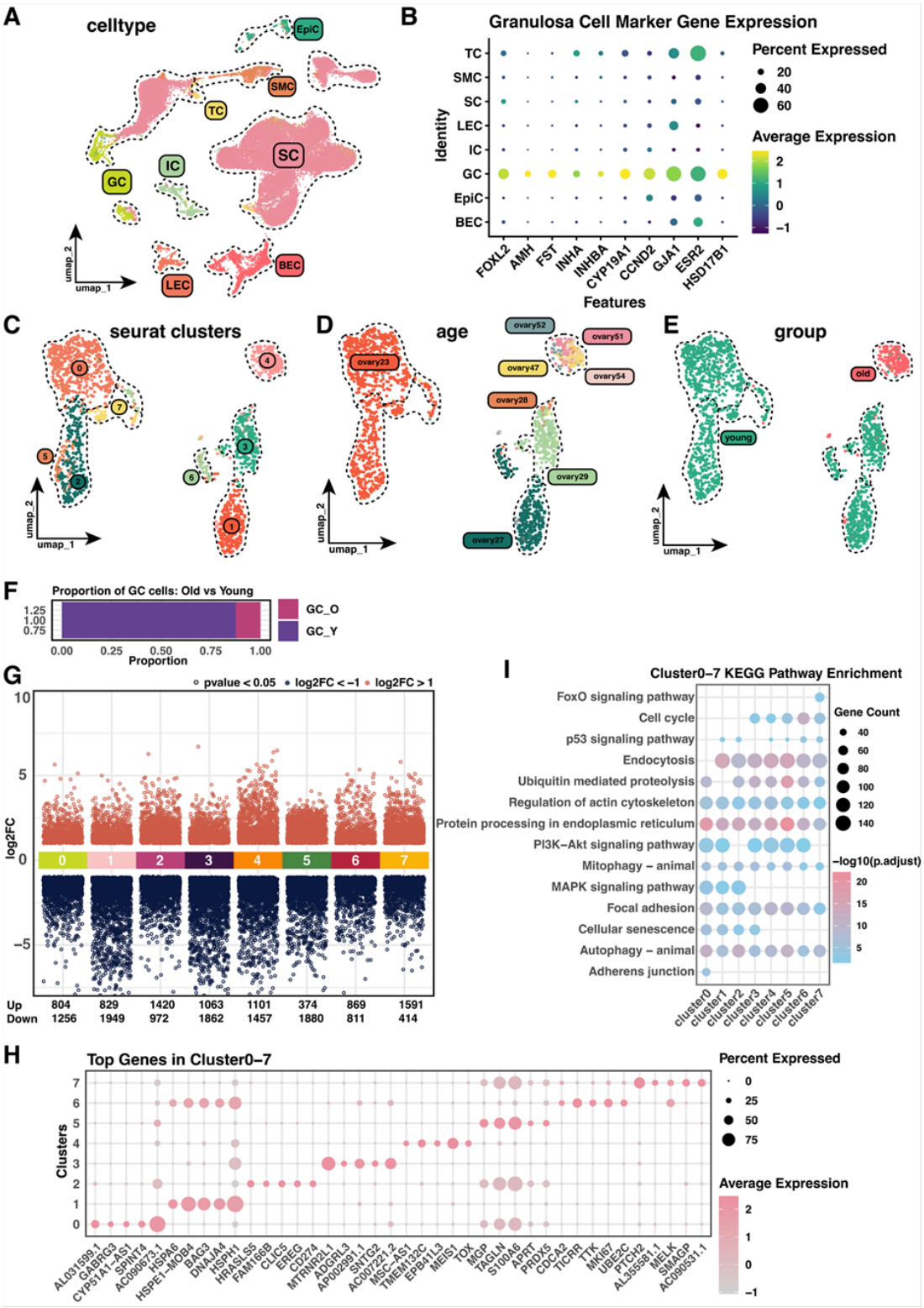


Figure 2

Single-cell transcriptomic analysis of ovarian granulosa cells (GCs) and subcluster characteristics.

A. UMAP visualization of cell types in GSE202601 snRNA-seq dataset, showing spatial distribution of major ovarian cell populations.

B. Dot plot of GC marker genes across all cell types, highlighting granulosa cell-specific expression.

C. UMAP of GC subclusters after extraction and re-clustering of granulosa cells using Seurat.

D. Age distribution of GC cells on UMAP, visualizing age-associated expression differences.

E. Group distribution (young vs. old) of GC cells on UMAP.

F. Proportion of GC cells in old and young groups, shown as stacked bar plots.

G. Differential expression analysis of 8 GC subclusters, identifying cluster-specific marker genes.

H. Dot plot of top 5 DEGs for each GC subcluster.

I. KEGG pathway enrichment of DEGs in each cluster, revealing potential biological functions.

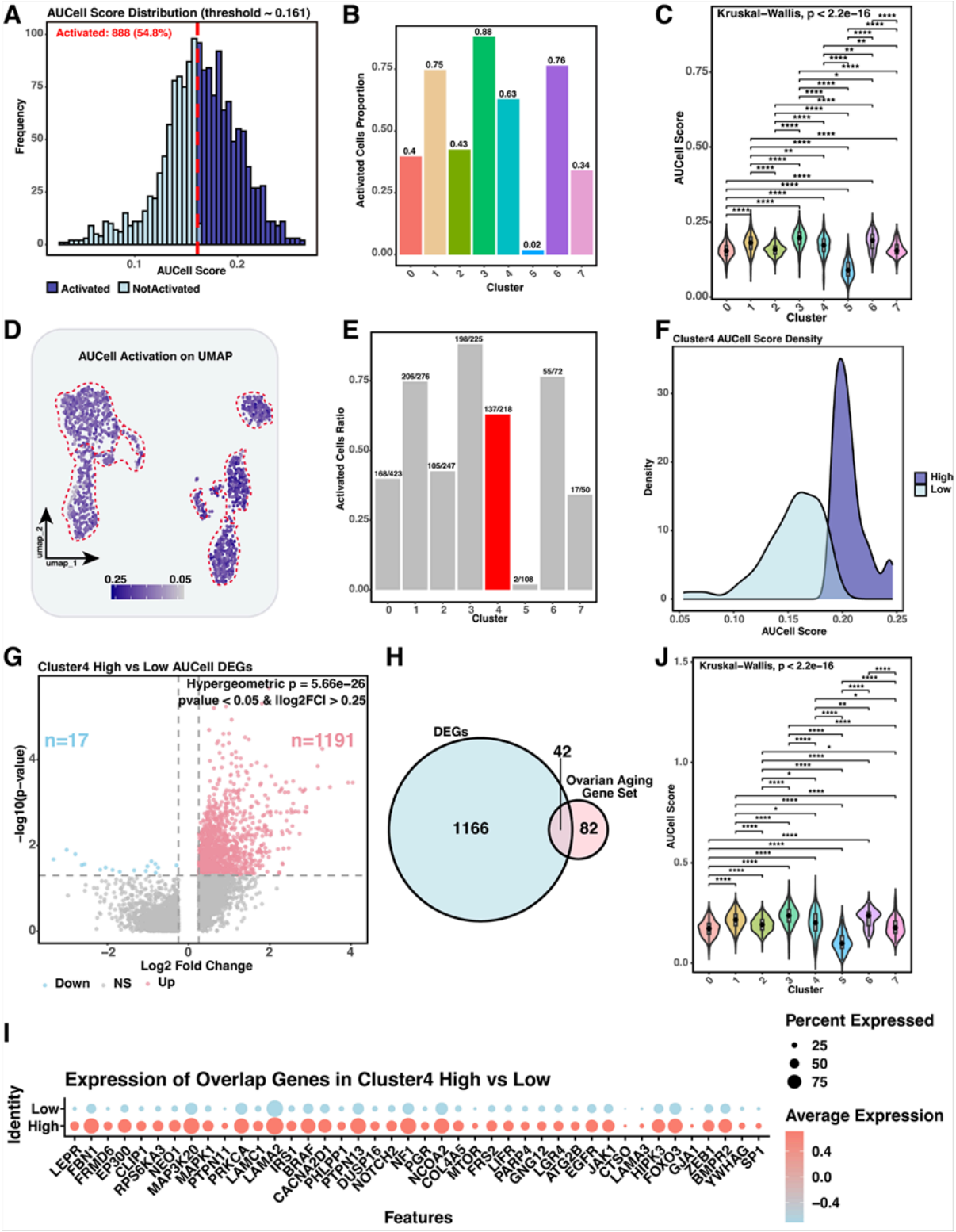


Figure 3

AUCell analysis of custom ovarian aging gene set and core gene characteristics in Cluster 4.

A. AUCell score distribution of 124 custom ovarian aging genes across all GC cells.

B. Proportion of activated cells in the 8 GC subclusters.

C. Statistical comparison of AUCell scores across clusters, with significance indicated.

D. Spatial distribution of AUCell scores on UMAP, color gradient from light blue to deep purple indicates low to high scores.

E. Activated cell proportion per cluster, with emphasis on Cluster 4.

F. Density plot of Cluster 4 AUCell scores, classifying cells into High and Low groups.

G. Volcano plot of DEGs between High vs. Low AUCell score cells in Cluster 4 (pink: upregulated, light blue: downregulated).

H. Venn diagram showing overlap between High vs. Low DEGs and 124 custom gene set, identifying 42 core genes.

I. Dot plot of 42 overlapping genes in High vs. Low AUCell score cells.

J. AUCell scores of 42 overlapping genes across 8 clusters, highlighting prominent activation in Cluster 4.

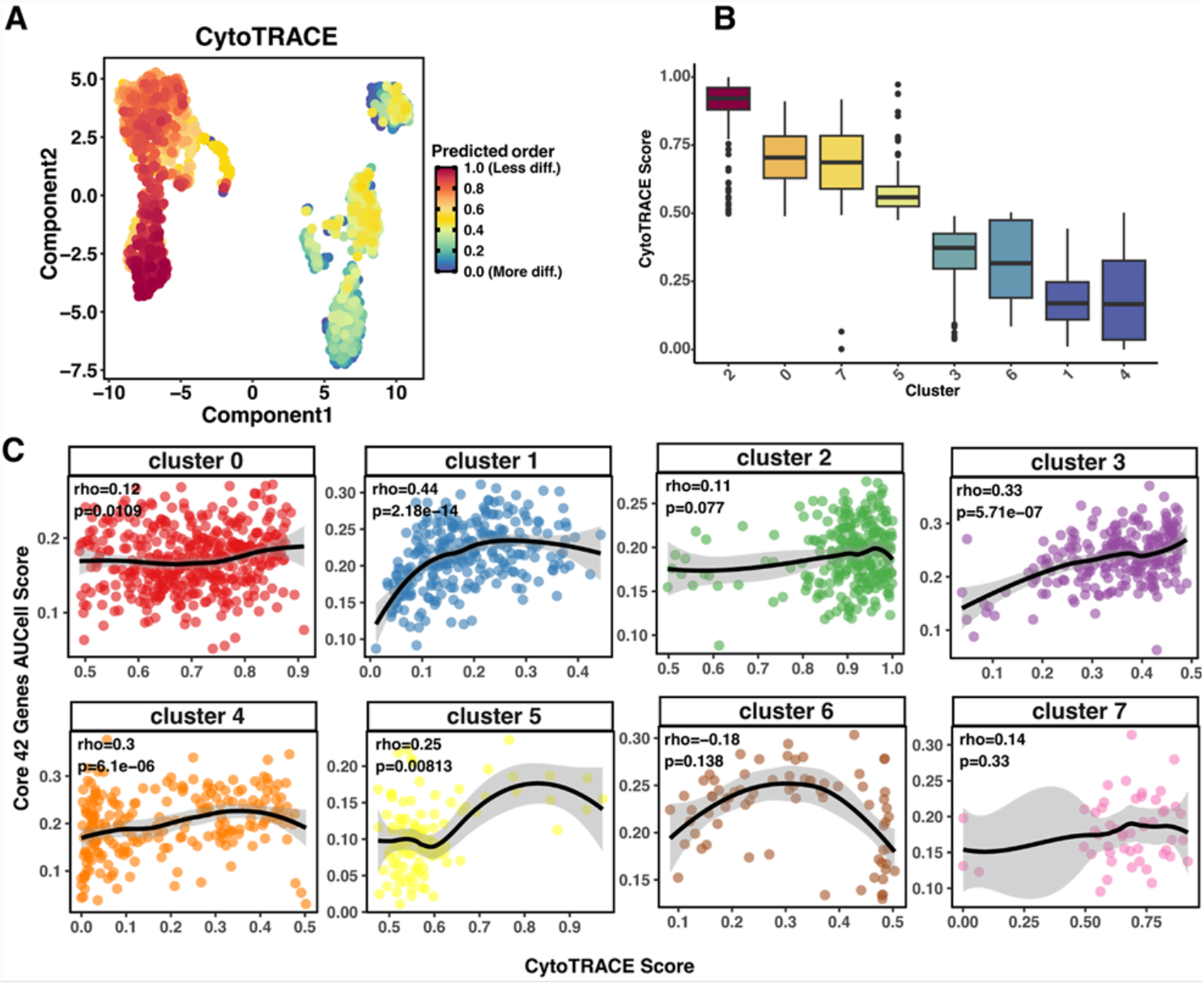


Figure 4

Developmental potential of GC cells and activation of core ovarian aging genes.

A. UMAP of CytoTRACE scores in GC cells, color gradient from light to dark indicates increasing developmental potential.

B. Boxplot of CytoTRACE scores across clusters, showing differences in developmental potential.

C. Correlation between CytoTRACE scores and AUCell scores of 42 core genes; Spearman correlation coefficient and significance indicated.

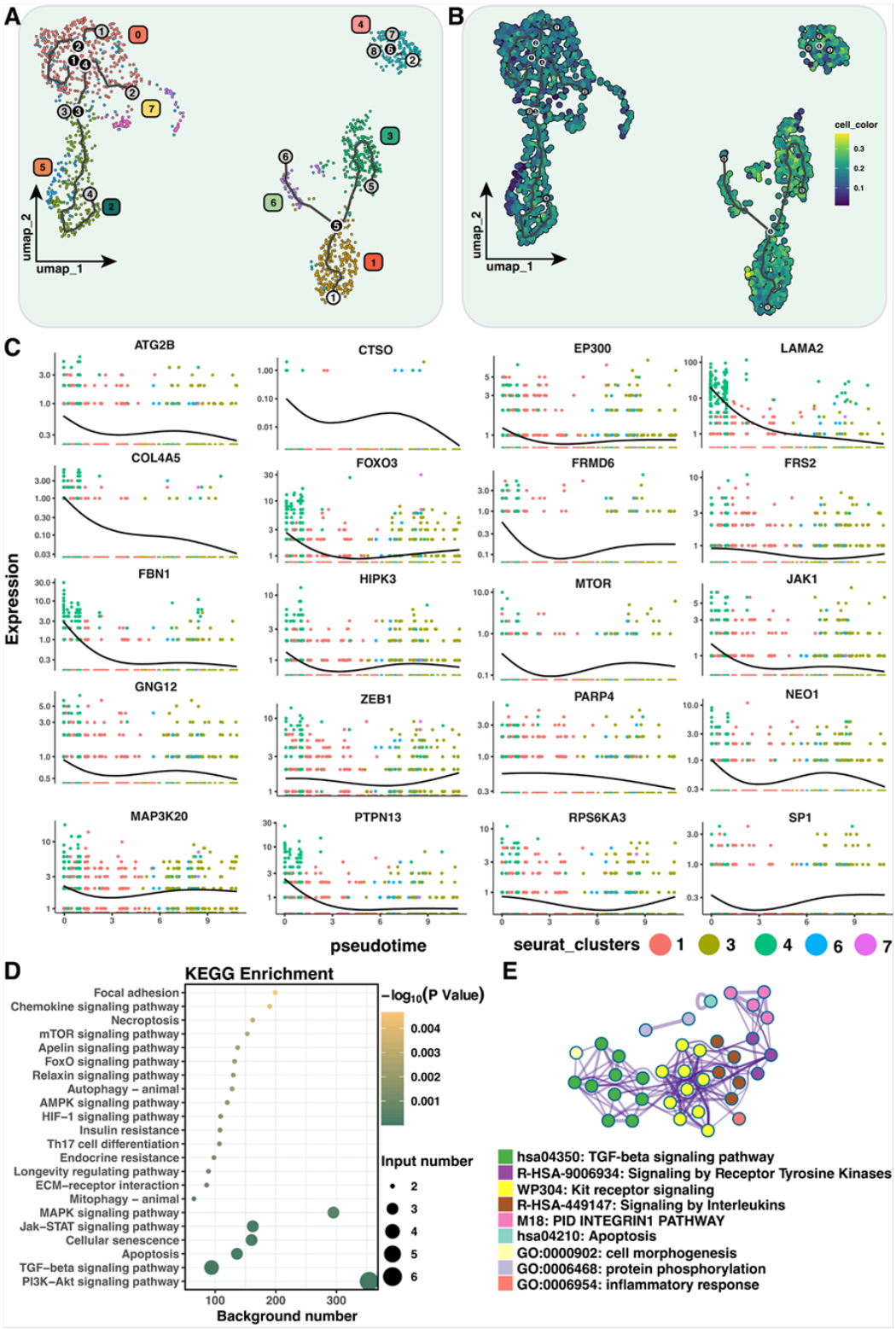


Figure 5

Pseudotime trajectory analysis and core gene activation in GC cells.

A. GC cell pseudotime trajectory constructed by Monocle3, visualized on UMAP.

B. AUCell scores of 42 core genes mapped onto pseudotime trajectory, yellow indicates higher gene activation.

C. Expression dynamics of 20 key genes selected from Cluster 4 along pseudotime.

D. KEGG pathway enrichment of the 20 key genes (significant pathways, $p < 0.05$).

E. Metascape analysis showing PPI network and key modules for the 20 genes.

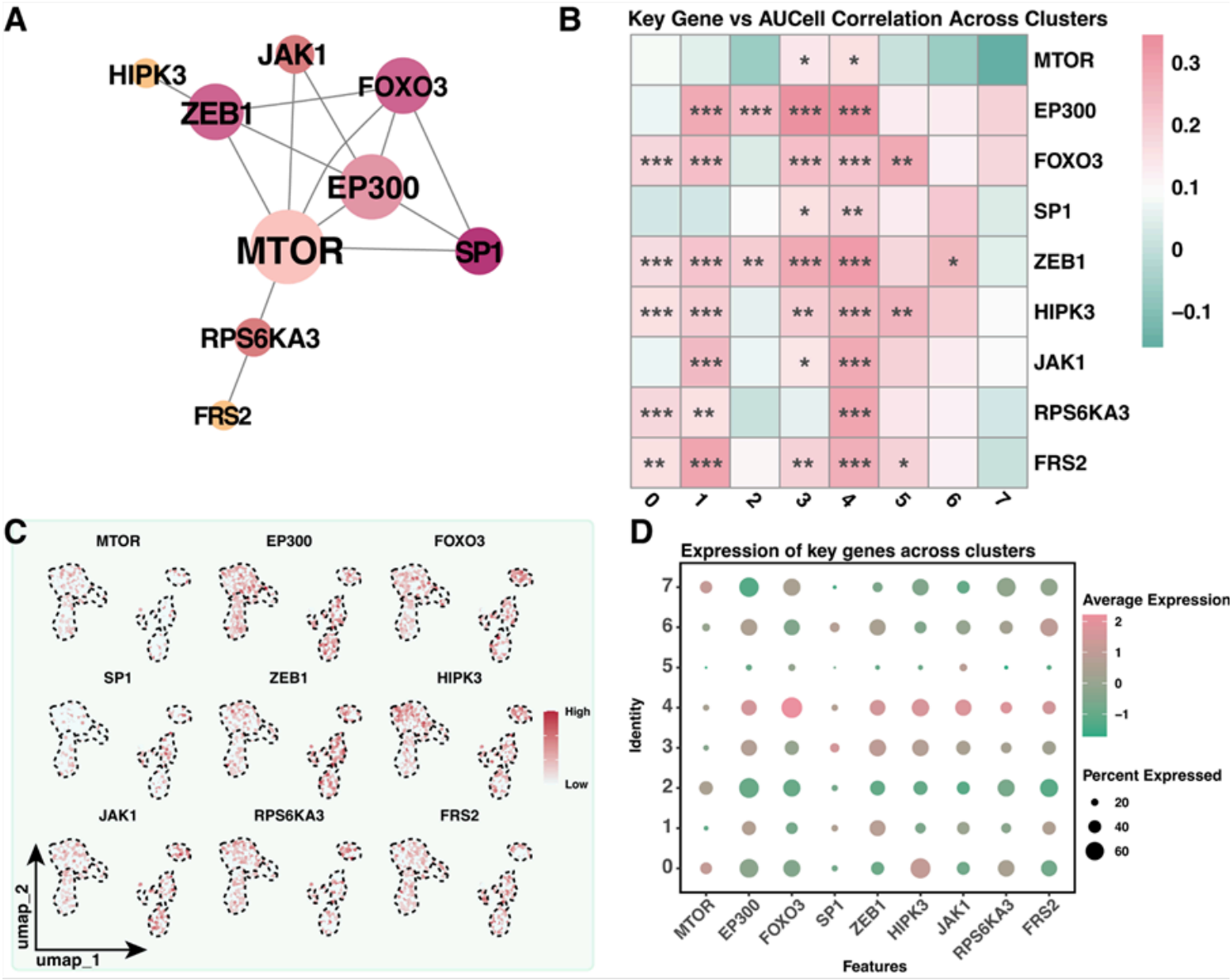


Figure 6

PPI and expression analysis of 9 core genes.

A. PPI network of 20 Cluster 4 key genes, displaying protein-protein interactions.

B. Heatmap of correlation between 9 core genes and AUCell scores of the 42 gene set across clusters (pink: positive correlation; green: negative correlation).

C. UMAP visualization of 9 core gene expression, deeper red indicates higher expression.

D. Average expression of 9 core genes across clusters, DotPlot representation (pink: high; green: low).

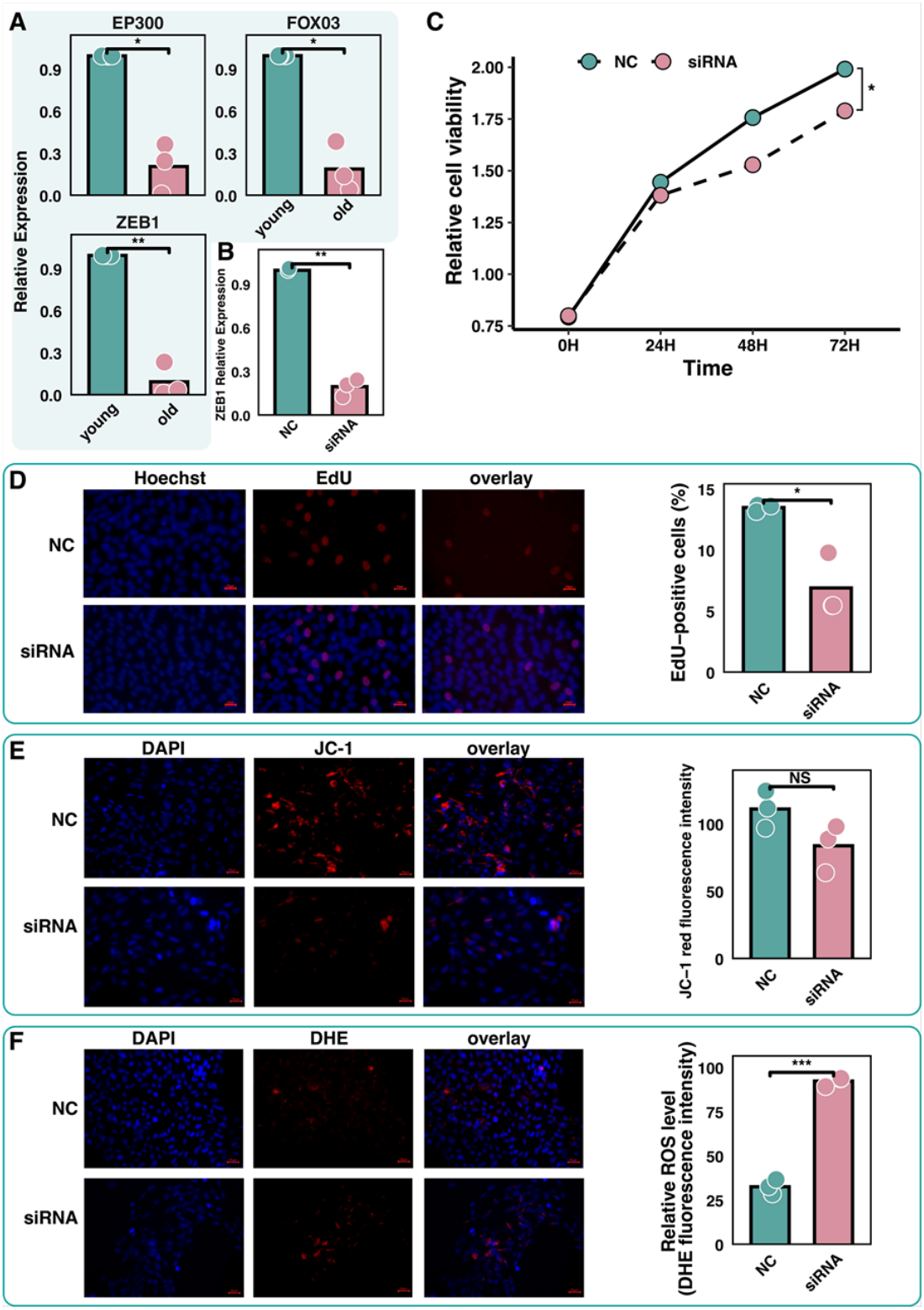


Figure 7

Validation and functional analysis of ZEB1 in ovarian granulosa cells.

A. qPCR validation of EP300, FOXO3, and ZEB1 expression in primary granulosa cells isolated from follicular fluid. Statistical test: Student's t-test (*P < 0.05, **P < 0.01).

B. qPCR verification of ZEB1 knockdown in granulosa cell line using siRNA.

C. CCK-8 assay showing effects of ZEB1 knockdown on GC proliferation (relative cell viability).

D. EdU staining for DNA synthesis and proliferation; left: representative fluorescence images (Hoechst, EdU, overlay); right: quantification of EdU-positive cells (%).

E. JC-1 staining assessing mitochondrial membrane potential; left: representative images (DAPI, JC-1, overlay); right: quantification of red fluorescence intensity.

F. DHE staining measuring intracellular ROS levels; left: representative images (DAPI, DHE, overlay); right: relative ROS intensity.

Supplementary Files

This is a list of supplementary files associated with this preprint. Click to download.

- Table1.xlsx
- SFigure1Figure1.tif